Toroidal-droplet instabilities in the presence of charge

Alexandros A. Fragkopoulos and Alberto Fernández-Nieves
School of Physics, Georgia Institute of Technology, Atlanta, Georgia 30332-0430, USA
(Received 8 October 2016; published 31 March 2017)

Neutral toroidal droplets can break via the surface-tension-driven Rayleigh-Plateau instability. They can additionally exhibit a shrinking instability, which is also driven by surface tension, whereby the handle progressively disappears. We find that charging a toroidal droplet can qualitatively change the behavior and cause the droplet to expand. We successfully model the transition from shrinking to expanding, considering the pressure balance across the interface of the torus. However, despite the change in behavior, charged toroidal droplets end up breaking into spherical droplets. We quantify how the wavelength of the fastest unstable mode associated to this breakup depends on the applied voltage and compare the results with theoretical expectations for charged cylindrical jets.

DOI: 10.1103/PhysRevE.95.033122

I. INTRODUCTION

The breakup of cylindrical jets has been the focus of study since the pioneering work of Plateau [1] and Rayleigh [2]. Periodic disturbances of the surface of a jet grow exponentially as long as the wavelength λ of the disturbance is greater than the circumference of the jet. The growth rate, however, depends on the perturbation wavelength via the dispersion relation, which is typically peaked. Hence, among all perturbations or modes, there is one which is the fastest and typically dominates the breakup process [3]. Recent work has shown that toroidal droplets are also unstable and break via the Rayleigh-Plateau instability [4,5] as long as the aspect ratio $\xi = R_0/a_0 > 2$, with R_0 and a_0 the radius of the central circle and the tube radius, respectively [see inset in Fig. 1(a)]. When $\xi < 2$, no unstable modes of the Rayleigh-Plateau type can grow and the toroidal droplet transforms into a sphere via a different mechanism. In this case the handle shrinks, eventually disappearing and resulting in a single spherical droplet [6]. Shrinking is present at all ξ, but it is the sole mechanism at low ξ for a torus to become a sphere. This instability is not observed for cylinders and it is intrinsic to the toroidal geometry [7–9]. Since the mean curvature H of the torus varies along its circular cross section, so does the Laplace pressure, $\Delta P = 2\gamma H$, with γ the surface tension. Shrinking then results from the fact that ΔP is smallest in the inside region of the torus and greatest in the outside region of the torus.

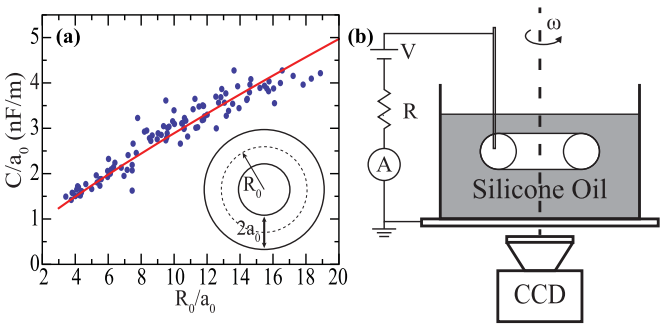

FIG. 1. (a) C/a_0 as a function of R_0/a_0. The line is a fit to Eq. (1), with ϵ_r as a free parameter. Inset: Schematic of a torus seen from below. R_0 is the radius of the central circle, shown with a dashed line, and a_0 is the tube radius. (b) Schematic of the experimental setup. A bath containing silicone oil rotates with an angular speed ω while the inner liquid is injected. The resultant toroidal droplet is charged at a voltage V, while the electrical current is measured. The subsequent evolution of the torus is captured from below using CCD camera.

Charge affects the dynamics of drops and jets. Zeleny [10] and, later, Taylor [11] studied the deformation of spherical droplets due to the presence of charge. They found that the interface transformed into a conical shape with a jet being ejected from its apex. These jets break axisymmetrically via Rayleigh-Plateau instabilities and are exploited in electrospray technology [12,13]. However, in this case, the wavelength of the fastest unstable mode is smaller than its value in the neutral case, and it decreases with increasing charge [14–18]. New phenomenology can also result from charging jets. Occurrence of whipping modes, which are unstable nonaxisymmetric modes driving the jet off-axis, is perhaps the most remarkable example [19]; these modes are exploited in applications like electrospinning [20–22]. Remarkably, both in electrospray and electrospinning the charged jet is not equipotential; the dynamics are so fast that the charges are unable to relax towards the interface, preventing control over the surface charge distribution.

In this article, we study the effect of charge on the evolution of toroidal droplets. On the one hand, surface charge introduces an electrical stress that competes with the stress due to surface tension, resulting in an expanding toroidal droplet at sufficiently high voltage; this is qualitatively different from the shrinking behavior seen in neutral toroidal droplets. On the other hand, and also in contrast to what is seen in the neutral case, charged toroidal droplets end up breaking into spherical droplets after expanding. This allows quantifying the effect of the charge on the Rayleigh-Plateau breakup of electrified jets. Note that in contrast to electrospray or electrospinning, in our experiments the torus is equipotential, allowing direct comparison with theoretical calculations where this is assumed.

II. EXPANSION OF CHARGED TOROIDAL DROPLETS

The generation of charged toroidal droplets is the same as in [6], with a small modification to incorporate charge. A glass cuvette with the outer liquid, silicone oil (30,000 cSt), is placed on top of a metallic rotating stage. As it rotates, the inner liquid, glycerol, is pumped through a metallic needle offset from the center of rotation inside the silicone oil. This

causes the formation of a curved jet, which closes onto itself and forms a toroidal droplet. The droplet is then charged by applying a voltage difference across the metallic needle and the rotating stage, as shown in Fig. 1(b). The sensitivity of our power supply is 10 V; as a result, this is the error in our voltage measurements. We monitor the current as a function of time and integrate to obtain the total charge Q. Once the toroidal droplet is charged, we remove the needle and image the droplet evolution from below using a CCD camera. We confirm the experimental procedure for charging and measuring Q using spherical droplets. For isolated spheres the relation between Q, the radius of the spherical droplet r, and the applied voltage V is well known: $V = Q/(4\pi\epsilon_r\epsilon_0 r)$, with ϵ_0 the vacuum permittivity and ϵ_r the relative dielectric constant of the outer liquid. Hence, the capacitance is $C = Q/V = 4\pi\epsilon_r\epsilon_0 r$. We confirm that Q is linear with V for constant r, and that C is linear with r. From a linear fit of the data, we obtain that $\epsilon_r = 4.6 \pm 0.4$.

For charged toroidal droplets, we measure Q at different V and obtain the capacitance. We do this for different aspect ratios and find that C/a_0 increases with increasing aspect ratio, as shown in Fig. 1(a). Theoretically, we solve Laplace's equation $\Delta\Phi = 0$, with Φ the electric potential, in a set of toroidal coordinates [23] using that $\Phi = V$ at the surface and that $\Phi \to 0$ at infinity [24]. The electric field can be obtained from the potential $\vec{E} = -\nabla\Phi$, and from the field we obtain the surface charge density, $\sigma = \epsilon_r\epsilon_0 E$, assuming a perfect conductor. By integrating σ over the surface of the torus, we can calculate Q [25], and using V, we obtain the capacitance [24]:

$$\frac{C}{a_0} = 8\epsilon_r\epsilon_0\sqrt{\xi^2-1}\sum_{m=0}^{\infty}(2-\delta_{0m})\frac{Q_{m-\frac{1}{2}}(\xi)}{P_{m-\frac{1}{2}}(\xi)}, \qquad (1)$$

where δ_{ij} is the Kronecker δ, and P_m and Q_m are the associated Legendre polynomials of the first and second kind, respectively, of order m. A fit of the data to Eq. (1), with ϵ_r as a free parameter, correctly captures the experimental results, as shown in Fig. 1(a). We obtain $\epsilon_r = 3.7 \pm 0.5$, consistent with our results for spheres and with the value of $\epsilon_r \approx 3$ reported for a similar silicone oil [26]. We note we can treat the torus as a perfect conductor since the charge relaxation time for glycerol is $\tau_r = \epsilon_0\epsilon_{r,g}/\sigma_g \approx 0.13$ ms, with $\epsilon_{r,g}$ and σ_g its relative dielectric constant and conductivity [27], respectively; this is about 5 orders of magnitude smaller than the typical time scale associated to the toroidal drop evolution. As a result, the electrical charge is able to relax to the interface, which can thus be treated as equipotential. In addition, experiments with a mixture of water and 16 mM sodium dodecyl sulfate, which is significantly more conductive than glycerol, showed no difference with those reported here.

The evolution of the charged toroidal droplet qualitatively changes compared to the uncharged counterpart. While for $\xi \approx 5.3$ and $V = 2$ kV the droplet shrinks, as shown in Figs. 2(a)–2(c), where we highlight the central circle at time $t = 0$ with a dashed line, for $\xi \approx 5.1$ but at a higher voltage of $V = 4$ kV the toroidal droplet expands, as shown in Figs. 2(d)–2(f). In addition, while the toroidal droplet breaks into three spheres in the first case, it breaks into four in the second case. This suggests that the wavelength of the fastest unstable mode is smaller for increasing charge, consistent with theoretical expectations [28]. We note that the black shadow in the upper part of Figs. 2(a) and 2(d) is due to the shadow from the holder of the injection needle, which we remove after the formation and charging of the torus.

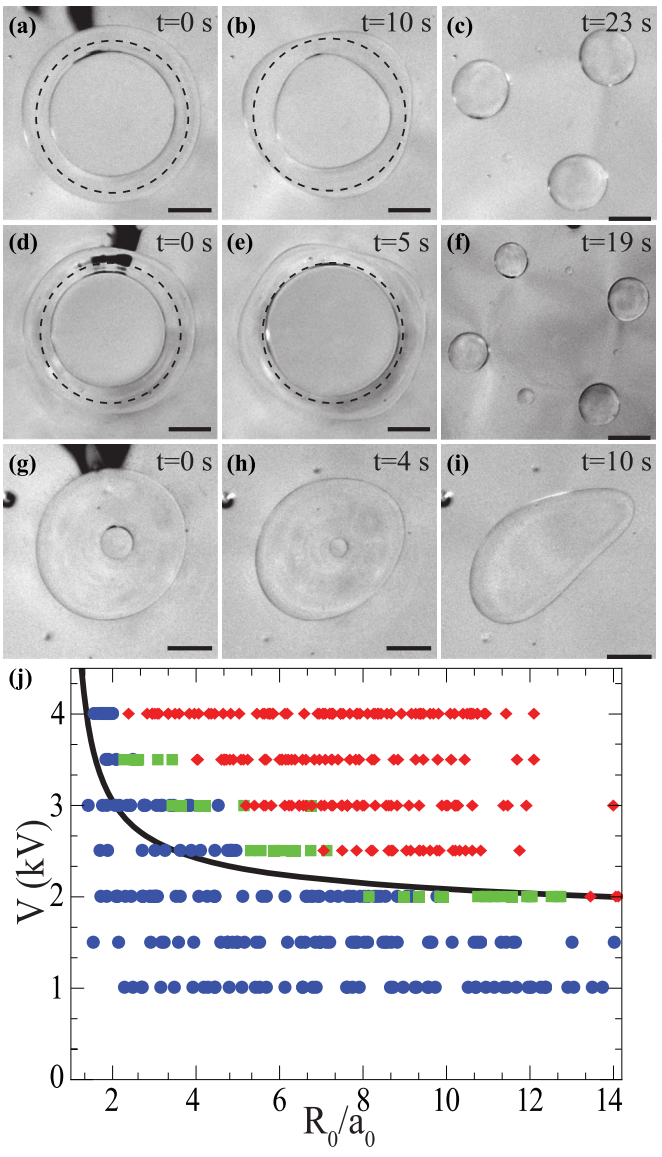

FIG. 2. Snapshots of the evolution of a torus with (a–c) $R_0/a_0 \approx 5.3$ and $V = 2$ kV, (d–f) $R_0/a_0 \approx 5.1$ and $V = 4$ kV, and (g–i) $R_0/a_0 \approx 1.6$ and $V = 4$ kV. The dashed circles in (a,b) and (c,d) correspond to the central circle at time $t = 0$. While in (b) the inner part of the torus has clearly shrunken, in (e) it has clearly expanded. The scale bar in all images is 2 mm. Note that the black shadow in (a), (d) and (g) is due to the holder of the injection needle. (j) Shrinking tori (circles), expanding tori (rhombus), and tori whose central circle remains stationary (squares) in a $V - \xi$ state diagram. The solid line is the theoretical transition line separating shrinking from expanding tori.

To model the transition from shrinking to expanding tori, we first consider the Laplace pressure of a toroidal interface, $2\gamma H$ [7]. This is plotted with a continuous line in Fig. 3 as a function of θ, the polar angle in the circular cross section of

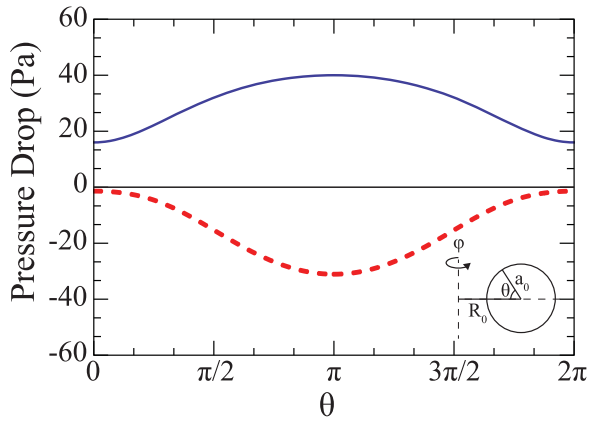

FIG. 3. Pressure drop across the interface of a torus due to surface tension (continuous line) and electrostatic stresses (dashed line) as a function of the polar angle θ. The inset is a cross section of the toroidal tube; the full torus is obtained by rotating along the φ direction. The values used for the calculation of the pressure drop are $a_0 = 1$ mm and $R_0 = 3$ mm ($R_0/a_0 = 3$), $\gamma = 32$ mN/m, and $V = 3$ kV.

the torus (see inset in Fig. 3). Note that the pressure inside the torus p at $\theta = \pi$ is greater than at $\theta = 0$. This pressure drop causes fluid to flow from the outside to the inside region of the torus, resulting in shrinking. Second, we consider the pressure drop across the interface due to the presence of charge, which is given by the Maxwell stress tensor for a perfect conductor $-\frac{1}{2}\epsilon_r\epsilon_0 E^2$, where E is calculated from Φ, and $\epsilon_r = 3.7$ as measured from the capacitance. In this case the pressure is maximum at $\theta = 0$ and it is minimum at $\theta = \pi$, as shown in Fig. 3 with a dashed line, exemplifying the fact that this electric stress is in direct competition with the Laplace pressure.

The total pressure drop across the interface of the torus is, hence, given by

$$p(\theta) - p_o = 2\gamma H - \tfrac{1}{2}\epsilon_r\epsilon_0 E^2, \qquad (2)$$

where p_o is the pressure outside the torus, assumed constant. Considering this simple pressure balance, we anticipate a shrinking-to-expanding transition when $p(\theta = 0) = p(\theta = \pi)$. We can recast this equality in terms of the applied voltage and the aspect ratio of the torus, as shown by the line in Fig. 2(j). We use $\gamma = 32$ mN/m, corresponding to the interfacial tension of our liquids measured using the pendant-drop method [29]. Above the transition line, the torus expands, while below the line, the torus shrinks. Note that the voltage required to transition from shrinking to expanding increases with decreasing ξ, illustrating that for sufficiently fat tori surface tension stresses dominate.

To test the expectations from our model, we experimentally explore the shrinking-to-expanding transition. We perform experiments with a constant injected volume of 0.05 mL and changed the applied voltage and the aspect ratio of the torus. We plot our results in a $V - \xi$ diagram, using circles for tori that shrink, rhombi for tori that expand, and squares for tori whose central circle remains unaltered. We find that the experiments follow the model predictions, particularly at high aspect ratio, as shown in Fig. 2(j). The deviations for lower aspect ratio are most likely due to the fact that the cross section of the toroidal droplets for high V and low

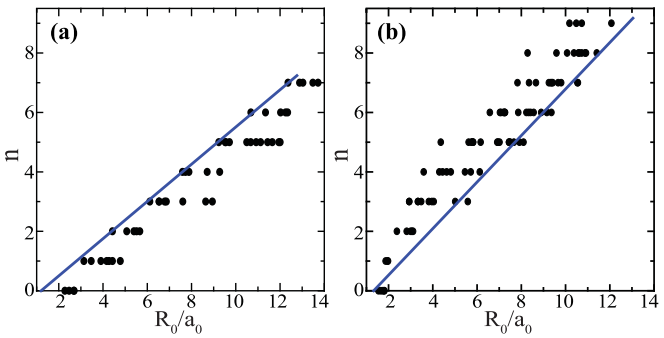

FIG. 4. Number of droplets n as a function of ξ for tori at (a) $V = 1$ kV and (b) $V = 4$ kV. In (a), all tori shrink, and thus we use the leftmost points of the steps to obtain the value of ka_0 associated to the fastest unstable mode. In (b), all tori expand, and thus we use the rightmost points of the steps to obtain this quantity.

ξ are not circular, as assumed by the model. This occurs because the pressure balance cannot be fulfilled everywhere on the torus; the electric stress is more sharply peaked than the Laplace pressure, as shown in Fig. 3. As a result, tori with a central circle that remains approximately stationary, still shrink near the handle and expand in the outer part of the torus, resulting in nonsymmetric deformations like those shown in Figs. 2(g)–2(i). Nevertheless, our simple pressure balance captures reasonably well the behavior seen experimentally.

III. BREAKING OF CHARGED TOROIDAL DROPLETS

Interestingly, when the drop expands, it always ends up breaking into spherical droplets. For cylindrical jets, theory predicts that the growth rate of a mode is a function of ka_0, where $k = \frac{2\pi}{\lambda}$ is the wave number of a given mode. Experimentally, the mode that dominates the breakup process is the mode that grows the fastest [3]. For a torus, we have periodic boundary conditions, and thus we expect a number of droplets n that depends on the number of wavelengths of the fastest unstable mode that we can fit inside a length equal to $2\pi R_0$. As a result, $n = 2\pi R_0/\lambda = ka_0\, R_0/a_0 = ka_0\,\xi$. We then expect that n is linear with ξ. However, n is a discrete variable, and as a result, plotting n versus ξ results in steps associated to a range of aspect ratios corresponding to the same n [6]; this is true irrespective of V. Our experiments illustrate this, as shown in Fig. 4 for two representative values of V. However, while for small V the behavior is dominated by shrinking, and thus the torus typically shrinks before it can fit an integer number of wavelengths of the fastest unstable mode, at higher V the torus typically expands before it can fit an integer number of wavelengths of the fastest unstable mode. Hence, to obtain the value of ka_0 associated to the fastest unstable mode, at different V, we use the leftmost points of the steps at low V, where the torus shrinks, and the rightmost points of the steps at high V, where the torus expands. Using these points, we confirm that n is linear with ξ, consistent with our expectations and as shown in Figs. 4(a) and 4(b). The slopes of the corresponding linear fits provide the value of ka_0 corresponding to the fastest unstable mode. We find that ka_0 increases with increasing V, as shown in Table I, and in qualitative agreement with theoretical predictions for

TABLE I. The fastest unstable mode ka_0 for different voltages obtained from experiments and theory.

V	ka_0	$(ka_0)_{\text{theory}}$
1.0 kV	0.59 ± 0.01	0.53
1.5 kV	0.60 ± 0.03	0.54
2.0 kV	0.63 ± 0.03	0.57
3.5 kV	0.79 ± 0.04	0.74
4.0 kV	0.85 ± 0.05	0.85

the breakup of electrified jets [17]. This indicates that λ decreases with increasing V and that breakup results in smaller droplets; this is indeed seen in Figs. 2(a)–2(c), where $V = 2$ kV and there are three drops after breakup, and Figs. 2(d)–2(f), where $V = 4$ kV and there are four drops after breakup.

To quantitatively account for the breakup results, we consider theoretical calculations for the evolution of charged viscous threads immersed in another viscous liquid [28]. The theoretical results depend on two parameters, $d = b/a$, where a is the radius of the jet, which is at $\Phi = V$, and b is the radius of a grounded cylindrical outer surface, and $N_E = \frac{\epsilon_r V^2}{2\gamma a_0}$, which is the electric Bond number accounting for the relative importance of electric stresses and Laplace pressure. To compare with our experiments, we choose d and N_E such that the electric stress in the theory is the same as the average electric stress on the surface of our tori. We find that the value of ka_0 corresponding to the fastest unstable mode increases with V and that the values are in reasonable agreement with our experimental results, as shown in Table I.

IV. CONCLUSIONS

We have shown that charge can qualitatively change the behavior seen for neutral toroidal droplets and cause the handle to expand. Additionally, and also in contrast to what is seen for neutral toroidal droplets, charged droplets always end up breaking via Rayleigh-Plateau instabilities, appropriately modified to account for the presence of charge. We account for the expansion with a simple model considering the pressure drop across a charged toroidal interface. It is the competition between surface tension and electrical stresses that determines whether a toroidal droplets shrinks or expands. The model treats the torus as electrostatically equilibrated, which is consistent with the small charge relaxation time compared to the characteristic time scale associated to the droplet evolution. This indicates the torus is equipotential. Since in the thin torus limit we can correctly think of the torus as a cylinder, slender electrified toroidal droplets can be seen as a model system with which to test instability theories for electrified jets. In this sense, charged toroidal droplets are advantageous compared to jets in electrospray, as these last ones are typically nonequipotential and have surface charge densities that, as a result, are hard to control and quantify. We believe our results open the way to additional work in electrohydrodynamics using toroidal droplets as a novel platform.

ACKNOWLEDGMENTS

We thank the National Science Foundation for financial support. We thank Ekapop Pairam for discussions on the experimental setup.

[1] J. A. F. Plateau, *Statique Exprimentale et Thorique des Liquides Soumis aux Seules Forces Molculaires* (Gauthier-Villars, Paris, 1873).
[2] L. Rayleigh, Proc. R. Soc. London **29**, 71 (1879).
[3] J. Eggers and E. Villermaux, Rep. Prog. Phys. **71**, 036601 (2008).
[4] J. D. McGraw, J. Li, D. L. Tran, A. C. Shi, and K. Dalnoki-Veress, Soft Matter **6**, 1258 (2010).
[5] H. Mehrabian and J. J. Feng, J. Fluid Mech. **717**, 281 (2013).
[6] E. Pairam and A. Fernández-Nieves, Phys. Rev. Lett. **102**, 234501 (2009).
[7] Z. Yao and M. J. Bowick, Eur. Phys. J. E **34**, 32 (2011).
[8] M. Zabarankin, O. M. Lavrenteva, and A. Nir, J. Fluid Mech. **785**, 372 (2015).
[9] M. Zabarankin, Proc. R. Soc. London, Ser. A **472**, 20150737 (2016).
[10] J. Zeleny, Phys. Rev. **10**, 1 (1917).
[11] G. Taylor, Proc. R. Soc. London, Ser. A **280**, 383 (1964).
[12] J. F. de La Mora, Annu. Rev. Fluid Mech. **39**, 217 (2007).
[13] R. T. Collins, J. J. Jones, M. T. Harris, and O. A. Basaran, Nat. Phys. **4**, 149 (2008).
[14] G. Taylor, Proc. R. Soc. London, Ser. A **313**, 453 (1969).
[15] D. A. Saville, Phys. Fluids **13**, 2987 (1970).
[16] A. Neukermans, J. Appl. Phys. **44**, 4769 (1973).
[17] R. T. Collins, M. T. Harris, and O. A. Basaran, J. Fluid Mech. **588**, 75 (2007).
[18] J. M. López-Herrera and A. M. Ganan-Calvo, J. Fluid Mech. **501**, 303 (2004).
[19] M. M. Hohman, M. Shin, G. Rutledge, and Brenner, Phys. Fluids **13**, 2201 (1994).
[20] J. Doshi and D. H. Reneker, J. Electrostat. **35**, 151 (1995).
[21] D. H. Reneker, A. L. Yarin, H. Fong, and S. Koombhongse, J. Appl. Phys. **87**, 4531 (2000).
[22] D. Li and Y. Xia, Adv. Mater. **16**, 1151 (2004).
[23] The set of toroidal coordinates used to solve Laplace's equation results from rotating the two-dimensional bipolar coordinate system (η, χ) along the azimuthal angle φ. Given a toroidal surface with R_0 and a_0, the bipolar coordinate system is defined using two focal points, $(x,z) = (\pm a_f, 0)$, where $a_f = \sqrt{R_0^2 - a_0^2} < R_0$. The coordinate χ is the angle between the two lines formed from a given point on the surface of the torus to the two focal points; it can take values $\chi \in (-\pi, \pi]$. A surface with a constant η defines a toroidal surface. If the surface of our tori is given for $\eta = \eta_0$, then $\cosh(\eta_0) = \xi$, with ξ the aspect ratio. Using this coordinate system, Laplace's equation is separable after writing the electrostatic potential as $\Phi = \sqrt{\cosh(\eta) - \cos(\chi)}\, H(\eta) X(\chi) \Phi(\varphi)$, where $H(\eta)$, $X(\chi)$, and $\Phi(\varphi)$ are single variable functions of η, χ, and φ, respectively.

[24] J. A. Hernandes and A. K. T. Assis, Phys. Rev. E **68**, 046611 (2003).

[25] The total charge is obtained from the surface charge density σ using toroidal coordinates. Then, $Q = \iint \sigma(\chi,\varphi) dA$, where the area element $dA = \sqrt{g_{\varphi\varphi} g_{\chi\chi}} d\varphi d\chi = a_f^2 \sinh(\eta_0)\, d\varphi d\chi / [\cosh(\eta_0) - \cos(\chi)]^2$, with g_{ij} the components of the metric tensor.

[26] W. Nol, *Chemistry and Technology of Silicones* (Academic Press, New York, 1968). The value of ϵ_r was measured at 100 Hz and is not the DC value relevant in our experiments. In addition, the molecular weight of the silicone oil is lower than what we use here. Both these effects will result in a slightly larger value of ϵ_r, which will more tightly agree with the values obtained from the measured capacitance.

[27] A. Barrero, J. M. Lopez-Herrera, A. Boucard, I. G. Loscertales, and M. Marquez, J. Colloid Interface Sci. **272**, 104 (2004).

[28] Q. Wang and D. T. Papageorgiou, J. Fluid Mech. **683**, 27 (2011).

[29] C. E. Stauffer, J. Phys. Chem. **69**, 1933 (1965).